J. COMBIN. MATH. COMBIN. COMPUT. 127a (2025) 7459--7478

Journal of Combinatorial Mathematics and Combinatorial Computing
www.combinatorialpress.com/jcmcc

Combinatorial Press

Calculation of the Number of Electric Vehicles Carried by Roll-on Roll-off Vessels Based on Fire Dynamics Simulation

Pan Shao[1,✉], Daowang Ren[2], Guoqi Ma[3]

[1] *China Waterborne Transport Research Institute, Beijing, 100088, China*
[2] *Shandong Gangtong Engineering Consulting Co., Ltd, Yantai, Shandong, 264000, China*
[3] *Rizhao Transportation Bureau, Rizhao, Shandong, 276800, China*

ABSTRACT

With the rapid development of the global cruise transportation industry and the worldwide increase of cruise ship transportation year by year, fire accidents on passenger and roll-on/roll-off ships (P/ROCs) pose a serious threat to economic properties. The article establishes a fire model of a passenger-roller ship carrying electric vehicles using the basic equation of dynamics, a large eddy simulation model, and a mixed fraction combustion model. The mesh division is used to improve the solving accuracy of the kinetic equations. The fire simulation conditions of the electric vehicle carried by a passenger-roller ship are designed to analyze the fire combustion characteristics of the passenger-roller ship transported in terms of wind speed, fire intensity, and ignition power in multiple dimensions using the FDS simulation software as a carrier. Based on the YOLOv5s network and combined with the improved non-great suppression algorithm, a statistical model for target detection of electric vehicles carried by a passenger-roller ship is designed, and the corresponding loss function is designed. When the external ambient wind speed was increased from 0.5 m/s to 6.5 m/s, the maximum temperature at the fire center of the electric vehicle carried by the passenger-roller ship was reduced from 883.93°C to 748.57°C. The improved YOLOv5s model has the highest mAP of 96.67% on the target detection of EVs after fire damage and an accuracy of 92.96% for counting the number of EVs after fire. The state of electric vehicles after fire damage can be obtained under fire dynamics simulation, and the target detection and quantity counting of electric vehicles can be effectively realized by combining deep learning technology.

Keywords: FDS, large eddy simulation model, combustion model, YOLOv5s, non-great suppression algorithm, passenger ship

✉ Corresponding author.
E-mail address: cxsp19860717@126.com (P. Shao).
Received 05 March 2024; Revised 20 April 2024; Accepted 05 December 2024; Published Online 15 April 2025.
DOI: 10.61091/jcmcc127a-413

1. Introduction

In the International Convention for the Safety of Life at Sea (SOLAS), a ro-ro ship is defined as a passenger ship with ro-ro premises or special premises, and a passenger ship is defined as a passenger ship providing accommodation for at least 12 passengers [1-2]. Roll-on/roll-off (Ro-Ro) ships are ships that usually travel short distances and have a combination of vehicle transportation and accommodation for passengers, and they are ships that have both Ro-Ro and passenger ship functions. Because of their ability to carry passengers and cargo at the same time, Ro-Ro ships are known as one of the most successful ship types in the shipping industry [3-6].

Roll-on roll-off (Ro-Ro) vessels have a low tolerance for accidents because of their ability to carry both passengers and cargo, and the number of passengers they carry is generally large [7-8]. In the passenger-roller transportation industry in recent years, the rate of ship accidents is high and the severity of the accidents is large, among which the accidental consequences of passenger-roller ship fires on human life and economic property are particularly serious [9-11]. Because the consequences of accidents on passenger-roller ships are generally very serious, the focus of research on the safety of passenger-roller transportation should be placed on the accident before it occurs and when it does not occur [12-14], to intervene in advance of the occurrence of accidents from the source, and to take measures to reduce the frequency of accidents, instead of taking measures to remedy the situation after the accident occurs [15-16]. And with the completion of new land and sea corridors in various regions, the passenger flow and cargo flow at sea will increase dramatically, which will lead to a continuous increase in the demand for passenger and roll-on/roll-off vessel capacity [17-19].

Complex structures, multiple fire types, high randomness, rapid spread, etc, characterize the fire accidents of passenger-roller ship-carrying electric vehicles. Clarifying the dynamics of their fire occurrence can help better clarify the economic losses caused by the fire. The article establishes the basic dynamic equations and the large vortex simulation model of the electric vehicle carried by a passenger-roller ship. It establishes the fire model of the electric vehicle carried by a passenger-roller ship in combination with the mixed fraction combustion model. The model meshing and independence verification were carried out by FDS software, and different working condition scenarios for the fire simulation of the passenger-roller ship were designed. Based on the simulation model, we analyzed the fire-influencing factors of EVs transported by passenger-roller ships. We explored the combustion characteristics of EV storage areas under different fire source powers. Taking the pictures of EVs after fire damage as the research data, a target statistical model that can be used throughout the transportation of EVs is constructed by combining the improved YOLOv5s network and the non-great suppression algorithm to realize the calculation of the number of EVs transported on passenger-roller ships.

2. Simulation Model of Electric Vehicles Carried by Roll-on Roll-off Vessels

With the rapid development of the global economy, the number of ships worldwide continues to increase. At the same time, the incidence rate of shipwrecks both at home and abroad remains high, among which the fire accidents caused by automobiles on passenger-roll-on/roll-off (PRO/ROO) ships account for a high proportion of shipwrecks, causing huge economic losses. Relying on the fire dynamics simulation FSD software, the simulation model of passenger-roller ship-carrying cars is established, and the changes in its fire parameters are deeply analyzed to support the understanding of the loss of passenger-roller ship-carrying electric cars in fires and to clarify the specific economic losses caused by fires on passenger-roller ships.

2.1. Fire Dynamics Basis and Simulation Steps

2.1.1. FDS simulation software implementation steps. Fire Dynamics Simulator (FDS) is a field simulation software based on the Stokes equations; the calculation method is different from other simulation software; a large area of space is divided into several cells, and parameters such as temperature, gas density, and concentration are calculated in the cell, and the movement of the gas is tracked through thermal radiation and turbulence phenomena in the fluid. There are two ways to deal with turbulent flow in FDS, i.e., the direct numerical simulation method and the large eddy Simulation. Large eddy simulation is a common method with higher efficiency and better accuracy than direct numerical simulation.

The fire simulation of electric vehicles carried by a passenger ship using FDS mainly consists of three processes, i.e., pre-processing, simulation calculation and post-processing, shown in Fig. 1 [20]. The pre-processing is mainly to establish the model by setting specific parameters, including the model size, determining the structure and layout of the passenger-roller ship carrying EVs, calculating the grid size, setting the pyrolysis parameters and combustion model, and determining the output variables.

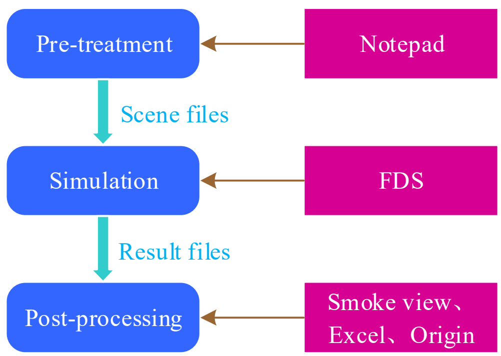

Fig. 1. Simulation Process and Tools

In addition to programming modeling directly in FDS, models can also be imported through other modeling software, such as the commercial modeling software Pyrosim and the open-source software Blender FDS and ACad2FDS. In this paper, we mainly build the scenario file through Pyrosim, i.e., the fire model of a passenger ship carrying an electric vehicle through Pyrosim. FDS mainly realizes the simulation calculation process, and during the calculation process, the relevant information of the calculation can be viewed through FDS, such as the heat release rate simulation time, etc. FDS realizes the post-processing.

Smokeview does the post-processing in FDS, which can directly display the smoke flow process and the temperature field change. If you need detailed result data to draw the relationship curve of each parameter with time, you need to use other plotting software, such as Tecplot, MATLAB, Origin, Excel, and so on. The post-processing of this paper is mainly with the help of Tecplot, Origin, and Excel-related software.

2.1.2. Controlling equations for fire dynamics. Numerical simulation of the fire combustion process of electric vehicles carried by passenger ships based on fire dynamics is theoretically based on the laws of conservation of mass, conservation of momentum, conservation of energy, and chemical reactions, which are universally established in nature and these laws can be mathematically organized into a set of basic equations, which are closed and solvable by combining the large-vortex simulation and the mixed-fraction combustion model.

The solution algorithm decomposes the fire field into many rectangular cells. The system of equations is used to calculate the gas density, velocity, temperature, pressure, and component concentrations within each cell. The spatial derivatives are approximated using the second-order central difference method. The second-order prediction-correction method is used to update each variable of the fluid. Numerical methods such as large vortex simulation are used to calculate heat radiation and fluid flow, to track and predict the generation and movement of the fire gases, and to calculate the growth and spread of the fire by combining with the mixed-fraction combustion model and the combustion characteristics of the passenger and roll-on/roll-off ship, to obtain the distribution of the parameters of the firing process such as the smoke, temperature, energy, and gas concentration in both space and time.

1) Basic Equations. FDS software is a computational fluid dynamics software developed for fire simulation, which uses numerical methods to solve the fire flow equations of a passenger-roller ship carrying an electric vehicle, mainly used for the numerical simulation of the smoke flow and heat transfer process in a fire [21]. The basic control equations solved by the FDS operation are as follows:

The continuity equation is:

$$\frac{\partial \rho}{\partial t}+\nabla\cdot(\rho u)=0 \tag{1}$$

where ρ is the density, t is the time, and u is the velocity vector.

The momentum conservation equation is:

$$\rho\left(\frac{\partial u}{\partial t}+\frac{1}{2}\nabla\cdot|u|^2-u\times_{\omega}\right)+\nabla p-\rho g=f+\nabla\cdot\tau \tag{2}$$

where f is the vector of external forces applied to the fluid, p is the pressure, τ is the viscous force tensor, ω is the vorticity, and g is the gravitational acceleration.

The component conservation equations are:

$$\frac{\partial}{\partial t}(\rho Y_i)+\nabla\cdot(\rho Y_i u)=(\rho D_i\nabla Y_i)+\dot{m}_i'' \tag{3}$$

where i is component i, Y_i is the concentration of component i, D_i is the diffusion coefficient of component i, and $\dot{m}_i''$ is the mass production rate of component i.

The energy conservation equation is:

$$\begin{aligned}\frac{\partial}{\partial t}(\rho h)+\nabla\cdot(\rho h u)&=\frac{\partial p}{\partial t}+u\cdot\nabla p-\nabla q_r\\&+\nabla\cdot(k\nabla T)+\sum_i\nabla(h_i\rho h D_i\nabla Y_i)\end{aligned} \tag{4}$$

where h is the specific enthalpy, q_t is the radiative flux, T is the temperature, and k is the thermal conductivity.

The equation of state is:

$$p_0=\rho TR\sum_i(Y_i/M_i) \tag{5}$$

where R is the gas constant and M is the relative molecular mass of the gas mixture.

2) Large eddy simulation model. In the fire dynamics model to simulate the fire of an electric vehicle carried on a roll-on/roll-off ship, a large eddy simulation is used to describe the turbulent mixing of the electrolyte vapors, combustibles such as O_2, and gaseous combustion products such as CO_2 and CO in a fire, and the turbulent mixing process determines the fire combustion rate. The basic idea of large

eddy simulation is to use direct numerical simulation (DNS) of large-scale turbulent motions and subgrid-scale models to simulate the effect of small-scale turbulent motions on large-scale turbulent motions.

In direct numerical simulations, the viscosity, thermal conductivity and substance diffusion coefficient are approximated from the theory of molecular motion. The kinetic viscosity coefficient μ_{DNS} of a multicomponent gas is expressed as:

$$\mu_{DNS} = \sum_l Y_l \frac{26.69\times10^{-7}\left(M_l T\right)^{1/2}}{\sigma_l^2 \Omega_v} \tag{6}$$

where σ_l denotes the Lennard-Jones rigid sphere diameter and Ω_v denotes the collision integral, which is an empirical function of temperature. The thermal conductivity k_{DNS} of the multicomponent gas is expressed as:

$$k_{DNS} = \sum_l Y_l \frac{\mu_l C_{p,l}}{\Pr} \tag{7}$$

where $C_{p,l}$ is the constant-pressure specific heat capacity of component l and the Prandtl number $\Pr = 0.7$. The substance diffusion coefficient $(\rho D)_{l,DNS}$ is expressed as:

$$(\rho D)_{l,DNS} = \frac{2.66\times10^{-7}\rho T^{3/2}}{M_{lm}^{1/2}\sigma_{lm}^2\Omega_D} \tag{8}$$

where component m is nitrogen, and $M_{lm} = 2\left(1/M_l + 1/M_m\right)^{-1}$, $\sigma_{lm} = \left(\sigma_l + \sigma_m\right)/2$, and Ω_D denote the diffusion collision integral, which is an empirical function of temperature.

In large eddy simulations, the subgrid size model is widely used as the Smagorinsky model, which simulates the dynamical viscosity as follows:

$$\mu_{LES} = \rho\left(C_S\Delta\right)^2\left(2\left(defu\right)\cdot\left(defu\right) - 2/3\left(\nabla\cdot u\right)^2\right)^{1/2} \tag{9}$$

where μ_{LES} denotes the turbulent viscosity used for subgrid-scale modeling in large eddy simulations, C_s is an empirical constant, Δ corresponds to the length of the grid cell size, and the term $defu$ is related to the discrete function, which represents the rate at which kinetic energy is converted to thermal energy.

The thermal conductivity k_{LES} and material diffusion coefficient $(\rho D)_{l,LES}$ are related to the turbulent viscosity μ_{LES} as:

$$k_{LES} = \frac{\mu_{LES} c_p}{\Pr} \tag{10}$$

$$(\rho D)_{l,LES} = \frac{\mu_{LES}}{Sc} \tag{11}$$

In the fire scenario of a passenger roll-on/roll-off vessel carrying an electric vehicle, it is assumed that both the Prandtl number $\Pr$ and the Schmidt number S_c are constants.

2.1.3. Mixed fraction combustion modeling of fires. The mixing fraction of component α in a mixture for a given control volume is the ratio of the mass of component α in the control volume to the total mass in the control volume. During combustion, the mixing fraction of certain components is a conserved quantity, usually defined as the mass fraction of the gas mixture in the fuel flow. Thus, the mixing fraction at the surface of the burner is 1 and in the fresh air is 0, while in the combustion zone the mixing fraction contains the residual fuel and the products of combustion of the fuel. The mixing fraction is a function of time and space and is generally expressed as a $Z(X,t)$ function.

It is assumed that when the fuel and oxygen are mixed, a chemical reaction occurs, which means that all components can be described by the mixing fraction, as shown in the following equation:

$$\begin{aligned} C_xH_yO_2Na_aM_b + v_{O_2}O_2 \rightarrow v_{CO_2}CO_2 + v_{H_2O}H_2O \\ + v_{CO}CO + v_2S + v_{N_2}N_2 + v_M M \end{aligned} \tag{12}$$

It is assumed in the chemical equation that the nitrogen in the fuel produces only nitrogen (N_2) during combustion, i.e., no oxides of nitrogen are produced (NO_x). For the reaction products of the other elements, their average molar masses are calculated and expressed in the molecular formula M, and it is assumed that these elements do not consume oxygen during the reaction, i.e., there is no elemental oxygen in M. Assuming that carbon soot is a compound made up of carbon and hydrogen atoms combined in a certain ratio, the stoichiometric coefficient v_s represents the amount of fuel converted to carbon soot and is related to the amount of carbon black y_s produced. v_s and y_s are related as:

$$v_s = \frac{W_F}{W_s} y_s, W_s = X_H W_H + (1 - X_H) W_C \tag{13}$$

where X_H is the mass fraction of hydrogen atoms in the carbon smoke, W_F is the molar mass of the fuel, W_C is the molar mass of carbon, W_H is the molar mass of hydrogen, and W_H is the molar mass of carbon smoke.

Similarly, there is a relationship between the stoichiometric coefficient v_{CO} and the amount of carbon monoxide produced y_{CO} as follows:

$$v_{co} = \frac{W_F}{W_{co}} y_{co} \tag{14}$$

The production of carbon monoxide and carbon soot is derived for well ventilated and late combustion, and their production is increased when the ventilation is poor, with the mixing fraction Z defined as:

$$Z = \frac{1}{Y_F^I}\left(Y_F + \frac{W_F}{xW_{CO_2}} Y_{CO_2} + \frac{W_F}{xW_{CO}} Y_{CO} + \frac{W_F}{xW_S} Y_S \right) \tag{15}$$

where Y_F^I is the mass fraction of fuel, at the fuel source, Y_F is the mass fraction of component α in the reaction, and x is the number of carbon atoms in the fuel molecule.

The passive conservation equation for the mixing fraction Z is:

$$\rho \frac{DZ}{Dt} = \nabla \cdot \rho D \nabla Z \tag{16}$$

where D/Dt is the follower derivative.

The combustion rate is assumed to be infinite, when the fuel and oxygen cannot coexist, defining the flame surface as:

$$Z(X,t) = Z_f = \frac{Y_O^\infty}{sY_F^I + Y_O^\infty}, s = \frac{v_{O_2}W_{O_2}}{v_F W_F}, v_F = 1 \tag{17}$$

where Z_f is the mixing fraction at the flame surface, Y_O^∞ is the mass fraction of ambient oxygen, and s is the theoretical amount of oxygen.

2.2. Establishment of numerical simulation model for Roll-on Roll-off (Ro-Ro) vessels

2.2.1. Modeling of fires on passenger-roller ship traffic. The research object of this paper is a large 7200-car-carrying automobile roll-on/roll-off vessel based on the deck flexible design concept, which has 13 vehicle decks in total, and the cabins are not provided with any transverse bulkheads in the direction of the ship's length. The hull is a longitudinal skeleton double bottom structure, with a traditional rigid design below the dry deck and a flexible design above the dry deck, and a row of pillars on each side of the hull, with the longitudinal and transverse spacing between the pillars of 12.5 m and 14.2 m. The fire model of the passenger-roller ship carrying electric cars in this paper is designed with a total of 13 vehicle decks, of which the third, fifth, seventh, and ninth layers are the Mobile vehicle deck; its stiffness is negligible, the other layers of the deck are fixed vehicle deck, among which the inner bottom plate and the sixth deck are watertight decks.

The seventh deck is watertight, full through deck for the large-scale passenger ship carrying cars with 7200 car seats. Based on the original design, this paper changes the deck structure into a rigid structure from the seventh deck upwards. In the model calculation of this paper, a total of multiple modeling scenarios are set up to study the effect of different fire conditions on the number of electric cars carried by the ro-ro ship by comparing the results of strength calculation under these multiple scenarios.

2.2.2. Delineation of Grids and Verification of Independence. The calculation area includes the deck space of the passenger ship where the fire may develop and spread, and the boundary of the calculation area of the opening part of the passenger ship should be extended outward by a distance of more than 1.5m to avoid the boundary affecting the flow of smoke in the opening part of the building and the external air supply. The upper part of the roof ridge of the passenger-roller shipbuilding is set up as a calculation area with a height of 1.8m to consider the calculation of smoke flow after the fire burns through the roof. The boundaries of the calculation area are open except for the bottom surface; and the simulated ambient temperature is 22℃, and the ambient pressure is $1.05*10^5$Pa.

Grid division determines the accuracy of the control equation solution; the finer the grid division is, the more accurate the simulation results are, but the computation time also increases exponentially. Therefore, the large-size FDS simulation must balance the accuracy and computational efficiency, different parts of the different size grid combination, and grid independence test.

For the fire plume model used in the large vortex simulation, the accuracy of the flow field calculation can be measured by the dimensionless expression D^*/δ_x, and a more satisfactory balance between simulation accuracy and computational efficiency can be achieved when the fire source characteristic diameter D^* is 4 to 16 times the minimum grid size δ_x, as verified in many studies. D^* is calculated from the heat release rate Q of the fire source. I.e:

$$D^* = \left(\frac{\dot{Q}}{\rho_\infty c_p T_\infty \sqrt{g}} \right)^{\frac{2}{5}} \tag{18}$$

where Q is the heat release rate of the fire source, ρ_∞ is the air density, c_p is the specific heat capacity of air, T_∞ is the ambient air temperature, and g is the gravitational acceleration.

Calculated that the passenger ship carrying electric cars burning fire source characteristic diameter of 0.55m, so take 0.135m for the key fire area grid size, that is, the deck area of the passenger ship, the rest of the area calculated grid size of 0.325m, and to meet the following grid division principles:

1) The size of any part of the model is not less than the grid width of the part.

2) The density of the grid near the fire source is larger, and the density of the grid away from the fire source is smaller, and the two neighboring grids must be aligned and the size conforms to the relationship of 2^n times.

3) A single calculation area within the model, its boundary and grid alignment or not less than two grid thickness, otherwise the calculation is reported as an error.

2.2.3. Fire Simulation Design for Rolling Stock Vessels. This paper establishes a model of a passenger ship carrying electric vehicles through FDS, aiming to study the change of the number of electric vehicles in the passenger ship in the event of a fire in the passenger ship carrying electric vehicles, and the safety distance between the air inlet of the fan and the air outlet of the smoke exhaust fan on the façade of the passenger ship under the circumstances of different locations of the fire source, different power of the fire source, and different winds in the environment. Above this safe distance, it is guaranteed that the fire smoke discharged by the smoke exhauster will not be re-absorbed by the air supply fan to cause "short-circuit reflux", which will jeopardize the life safety of the people escaping from the building.

In this paper, the simulation of the passenger ship carrying electric vehicles model fire mainly centers on the location of the fire source when the fire occurs, the power of the fire source, and the ambient wind, three uncertain factors. Three typical locations are selected for the fire start location, i.e., high-rise fire source location (11 to 13 floors), mid-rise fire source location (5 to 10 floors), and low-rise fire source location (1 to 4 floors). The fire source power is divided into three: the fire source power is 2.2MW when the sprinkler system starts normally, the fire source power is 8MW when the sprinkler system fails, and the ambient wind is divided into ambient wind and no ambient wind, which the ambient wind is selected as the annual average wind speed and the most unfavorable wind direction (i.e., the exhaust port is in the wind direction upstream of the air inlet). This paper mainly selects the test equipment as a co-detector, a total of nine measurement points. The measurement points are mainly uniformly arranged in the cross-section of the outdoor duct opening of the mechanically pressurized air supply fan. The above three factors are controlled separately to adjust the spacing between the air inlet of the air supply fan and the air outlet of the smoke exhaust fan, and the data obtained from the co-measurement points are used to judge the safe spacing between the air supply and air outlet.

3. Simulation analysis of electric vehicle fire carried by a passenger-roller ship

With the continuous development of the social economy, the automobile transportation industry relying on roll-on/roll-off ships is developing rapidly. However, the battery transportation of electric vehicles is a high-risk factor of fire, which leads to the frequent occurrence of ship fire accidents and seriously threatens the life safety of the crew and the property safety of electric vehicles. In this chapter, based on the previously designed model of an electric vehicle transported by a passenger-roller ship, FSD software is used to simulate and analyze the fire process and to understand the change of fire dynamics of an electric vehicle transported by a passenger-roller ship.

3.1. Factors affecting fires carried by roll-on/roll-off passenger ships

3.1.1. Impacts of wind speeds. Based on the simulation model of the electric vehicle carried by a passenger-roller ship given in the previous section, the fire changes of the electric vehicle carried by a passenger-roller ship under different wind speeds are investigated, and four different sizes of wind conditions are set, i.e., the wind speeds are 0.5 m/s, 2.5 m/s, 4.5 m/s and 6.5 m/s, respectively, and the position of the flame influence deviates out of the computational domain when the wind speed is too large, and it will not be discussed again. All variables except wind speed were set to default values, and the data for each condition were extracted after simulating the fire for 2 hours. The temperature field of the bottom plate of the EV storage area of the passenger ship under different wind speeds is shown in Fig. 2.

From the figure, it can be seen that the influence of increasing wind speed on the temperature field of the fire model of the passenger and ro-ro ship carrying electric vehicle is mainly characterized by the temperature center shifting with the wind direction and the shift distance increases with the increase of wind speed. As the wind speed increases, the center's maximum temperature decreases by a small amount. When the wind speed of the external environment is 0.5m/s, the maximum temperature at the center of the fire of the passenger ship carrying an electric vehicle can reach 883.93℃, and when the wind speed of the external environment is 6.5m/s, the maximum temperature still has 748.57℃. As the wind speed of the outside environment becomes larger, there is no obvious effect on the flame range of the passenger roller, and the high temperature range is constantly spreading, but the overall decrease is smaller.

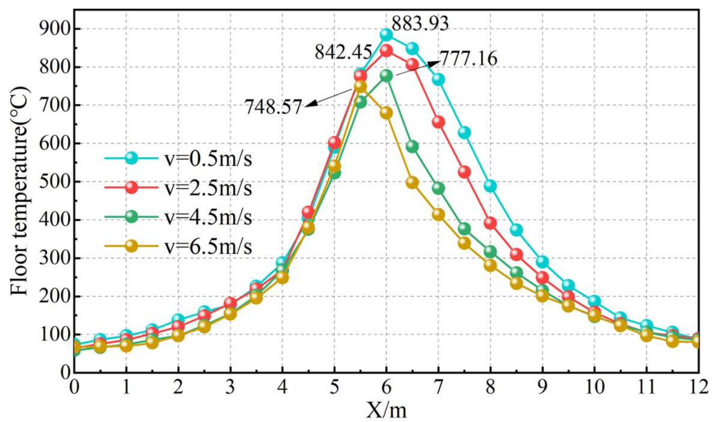

Fig. 2. The wind speed is affected by the fire of the passenger roller

3.1.2. Effects of fire intensity. After clarifying the influence of the external ambient wind speed on the fire of the passenger roll-on/roll-off ship carrying electric vehicles, this paper sets up four different working conditions, i.e., the fire intensity of 12, 14, 16, and 18 MW fire intensity, respectively. Combined with the kinetic equations given in the previous section, the temperature field variations along the centerline of the ro-ro ship under different fire intensities were calculated using FSD software, as shown in Fig. 3. From the figure; it can be seen that the influence of fire intensity on the fire temperature field of the passenger roll-on/roll-off ship carrying EVs is mainly reflected in the maximum temperature and the influence range. As the flame intensity gradually becomes larger, the maximum temperature at the center increases continuously, from 486.83°C to more than 932.76°C, while the range of fire influence also gradually expands. It can be seen that eliminating the source of fire is an important fire prevention measure. Restriction or strengthening of norms to guide the passenger roll-on/roll-off ship to carry electric cars and other vehicles that are easy to cause high-intensity fire fire fire measures prohibit the accumulation of firewood, grass, garbage, and other flammable materials in the passenger roll-on/roll-off ship, a series of measures can effectively reduce the destruction of fire on the deck of the passenger roll-on/roll-off ship.

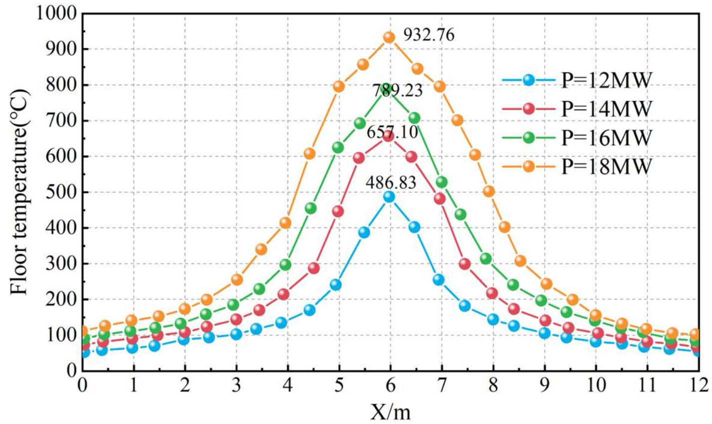

Fig. 3. Temperature field changes under different fire intensity

3.2. Combustion characteristics at different ignition powers

3.2.1. Effect on flue gas temperature. After understanding the factors that influence the fire of the electric vehicle carried by the passenger-roller ship, this paper sets up four fire conditions under different fire source powers to study the fire combustion characteristics of the electric vehicle storage area with different fire source powers. When the fire source power is 200, 400, 600, and 800 kW, the influence on the smoke layer temperature is shown in Fig. 4.

As can be seen from the figure, the smoke layer temperatures under different fire source powers all experienced a first increase and then a rapid decrease. The higher the fire source power, the larger the peak of the smoke layer temperature and the earlier the downward trend appears, and when the fire source power reaches 800kW, the peak of the smoke layer temperature can reach 357.88℃. The decrease in the smoke layer temperature may be related to the insufficient oxygen content in the chamber. The study showed that when the oxygen volume fraction was lower than 14%, the combustion was inhibited and quenched quickly. Then, there was no hot smoke replenishment, which decreased the smoke layer temperature. Meanwhile, under the condition of having openings, the smoke from the fire compartment will spread to other compartments through the openings, leading to a further decrease in the smoke layer temperature.

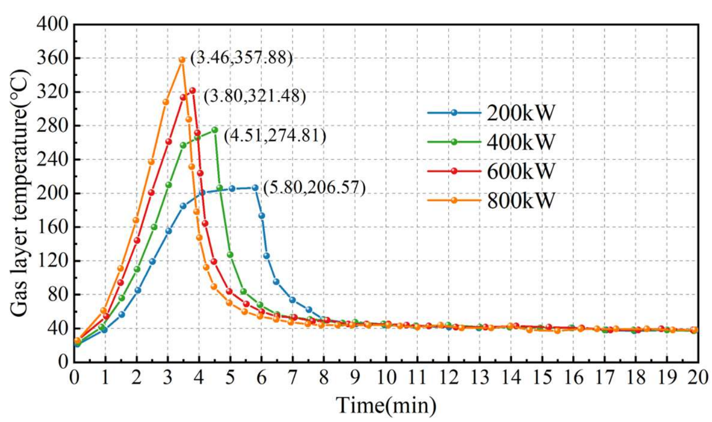

Fig. 4. The effect of the temperature of the smoke layer

The changes in oxygen content and actual firepower in the fire chamber under the same working condition are shown in Fig. 5, of which Fig. 5(a)~(b) shows the changes of oxygen content and actual firepower, respectively. As can be seen from the figure, the rate of decrease of oxygen content in the chamber is positively correlated with the fire source power, i.e., the higher the fire source power, the faster the oxygen consumption. Under different fire source powers (in decreasing order of 800kW), the time for the oxygen volume fraction to fall to 14% is 3.95, 4.01, 4.89, and 6.12min, respectively, which is very close to the time node of the sudden decrease of the temperature of the flue gas layer under different fire source powers. This is because when the oxygen volume fraction decreases to 14%, the combustion is inhibited and quenched rapidly, which leads to a sudden decrease in the flue gas layer temperature. When the power of the fire source is higher, the oxygen volume fraction's drop to 14% is shorter, and the flue gas layer temperature shows a decreasing trend earlier. In addition, the ignition source power under each operating condition increased in 0~8 min, reached the maximum value around 8 min, and then entered the stable combustion stage. However, due to the different times for the oxygen concentration to drop to 14% under different ignition power, the period of stabilized combustion for different ignition power is also different. In summary, under the same conditions, the higher the fire source power, the faster the temperature of the flue gas layer rises, the larger the temperature peak of the flue gas layer, and the earlier the downward trend occurs. Under the same conditions, the higher the power of the fire source, the more rapid the oxygen consumption, and the higher the power of the fire source, the earlier the extinguishing time without intervention.

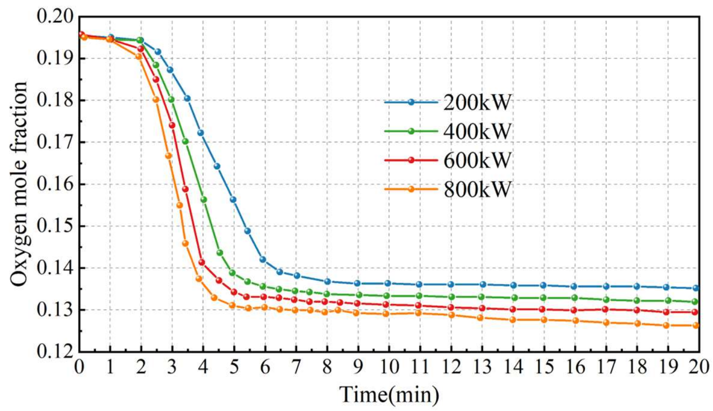

(a) Oxygen content

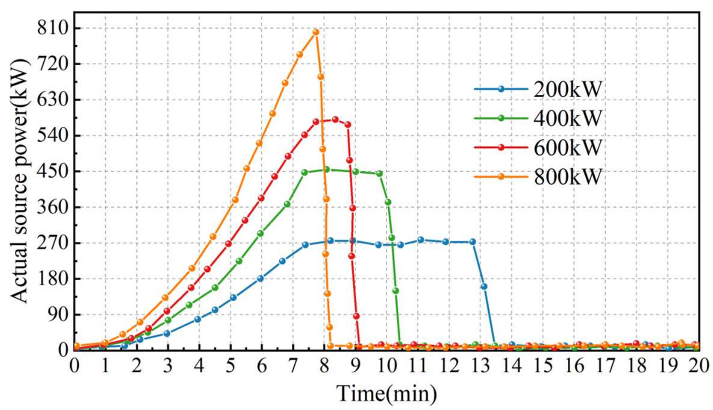

(b) Actual source power change

Fig. 5. Oxygen content and actual source power change

3.2.2. Effect on air-layer temperature. Based on the simulated working conditions of the passenger ship carrying electric vehicle model set up in the previous section, the air layer temperature changes under different fire source powers are calculated as shown in Fig. 6. As can be seen from the figure, the overall regularity of the air layer temperature under different fire source powers is similar to the effect of different fire source powers on the smoke layer temperature. The larger the fire source power, the larger the peak air layer temperature and the earlier the downward trend appears, and when the fire source power reaches 800kW, the peak air layer temperature can reach 144.0℃. Under the same conditions, the fire source power is positively correlated with the air layer temperature in the chamber, i.e., the higher the fire source power is, the higher the air layer temperature is, and the earlier the time of the downtrend point appears. This is related to the decrease in oxygen concentration, leading to the extinction of the fire source.

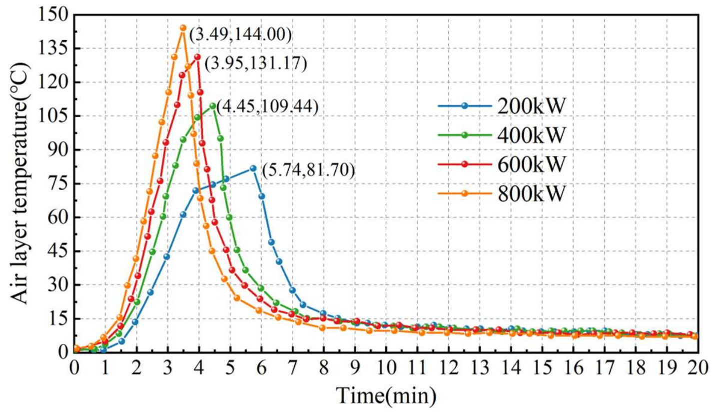

Fig. 6. The effect of the air layer temperature

4. Statistics on the target number of electric vehicles carried by roll-on/roll-off vessels

Cross-sea passenger roll-on/roll-off ships combine the characteristics of passenger ships and roll-on/roll-off ships and have the advantages of high loading and unloading efficiency, fast ship turnover, direct land and water access, and convenient intermodal transportation. However, in sharp contrast to the great commercial success of ro-ro ship transportation, vicious maritime accidents on ro-ro ships have occurred frequently, especially fires occurring on ro-ro ships carrying electric cars, which can lead to great loss of life and property, causing a bad impact on society. To clarify the loss of electric vehicles carried by passenger-roller ships under fire, this paper takes the images of electric vehicles carried by passenger-roller ships under fire. It adopts the deep learning method for detecting electric vehicles after fire, which supports the inventory of economic losses caused by fires in electric vehicles carried by passenger-roller ships.

4.1. Deep Learning Based Statistical Modeling of Automotive Targets

4.1.1. Target detection based on YOLOv5s. The YOLOv5s network structure is shown in Fig. 7, which is mainly divided into Input, Backbone network, Neck network, and Head output. The input side mainly carries out the processing of the input image, the Backbone network extracts features from the input image, the ECAShuffle-Net is used as the backbone network, the Neck network fuses the feature information extracted by the Backbone network, and finally the Head output outputs the detected results [22].

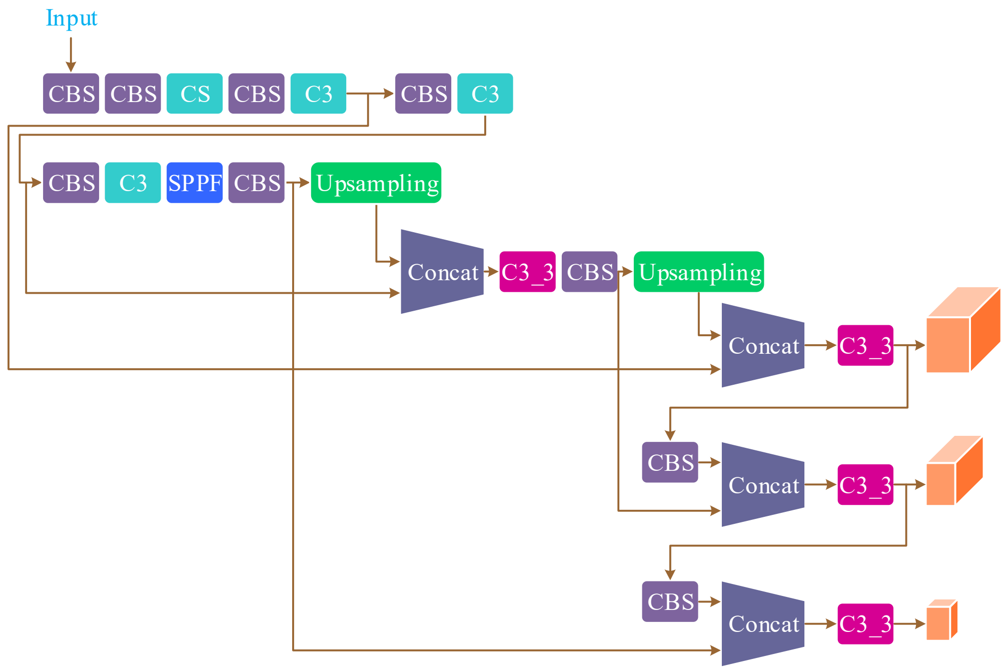

Fig. 7. Electric vehicle target detection based on YOLOv5s

1) Inputs. For different datasets, first, the anchor frame sets the initial length and width values, and then the network outputs the predicted frame based on the initial anchor frame. Then, the network center coordinates and width-height offset are calculated by comparing them with the real frame. Finally, by updating the network parameters in reverse during the iteration process, the training efficiency of the model can be significantly improved. The detection dataset of this paper mainly comes from the thermal map data of EVs carried by passenger ships after the fire dynamics simulation in the previous section, and a total of 428 fire images are acquired, which are used in the statistics of the number of EVs in the later section.

2) Feature extraction network. The CBS module comprises Conv, BN layer, and SiLU activation function. The BN layer's most important role is to accelerate the network's convergence speed with some regularization effect. The BN layer first calculates the mean μ and variance among all the elements within an Input Feature $(x_1 \cdots x_i)$, and then subtracts x_i from the elemental count to arrive at the mean value. This is then divided by the standard deviation and finally the final output y_i is computed by performing affine transformation operations on the learnable parameters γ and β. i.e.:

$$\mu_B \leftarrow \frac{1}{m}\sum_{i=1}^{m} x_i \tag{19}$$

$$\sigma_B^2 \leftarrow \frac{1}{m}\sum_{i=1}^{m}\left(x_i - \mu_B\right)^2 \tag{20}$$

$$\hat{x}_i \leftarrow \frac{x_i - \mu_B}{\sqrt{\sigma_B^2 + \varepsilon}} \tag{21}$$

$$y_i \leftarrow \gamma \hat{x}_i + \beta \equiv BN_{\gamma,\beta(x_i)} \tag{22}$$

The SiLU activation function is a smooth non-monotonic function, which, like the ReLU activation function, has no upper bound and thus no gradient saturation problem.

The SiLU activation function and the derivative function are formulated as:

$$SiLU(x) = x \cdot Sigmoid(x) = \frac{x}{1+e^{-x}} \tag{23}$$

$$SiLU'(x) = \frac{1+e^{-x}+xe^{-x}}{\left(1+e^{-x}\right)^2} \tag{24}$$

3) Feature Fusion Network. The Neck network structure in YOLOV5s adopts the feature pyramid network (FPN) and path aggregation network (PAN) structure between the backbone network and the outputs. The FPN transmits the feature information in a top-down manner, adding the high-level semantic information and the shallow semantic information one by one to improve the ability to express multi-scale semantics. The PAN structure is based on the FPN in a bottom-up manner feature fusion, which integrates shallow localization information into deep features and improves the ability to express features at different scales. Combining these two structures strengthens the network's target localization ability and the accuracy of target recognition.

4) Output. The Head part of YOLOv5s is mainly used for detecting targets and outputs feature maps of 30 × 30, 60 × 60, and 90 × 90, respectively. In the Head part of YOLOv5s, the feature maps of various sizes obtained from the Neck are expanded with a convolution of 2 × 2 on the number of channels, and the number of channels of the expanded features is (number of categories + 5) × number of anchors per detection layer. The Head part of YOLOv5s, with a convolution of 2 × 2 on the number of channels, is expanded to (number of categories + 5) × number of anchors per detection layer. The four detection layers in the Head correspond to the three different sizes of feature maps obtained in the Neck. Four anchors with unequal aspect ratios are preset on each grid of the feature map for target prediction and regression.

4.1.2. Improvement of the non-great suppression algorithm. The non-Maximum Suppression (NMS) algorithm is an important part of the target detection algorithm and is used to select the prediction frame closest to the true frame. The NMS algorithm first sorts the prediction frames from highest to lowest according to the confidence score, retains the highest scoring prediction frame, and removes the other prediction frames with an overlap area with this frame greater than a certain threshold value [23]. The process is performed for all the remaining prediction boxes, where the overlap area is calculated using CIOU.

In the fire scenario of a passenger ship carrying electric vehicles, there is often some overlap and occlusion between vehicles, and the NMS algorithm used in YOLOv5 is not able to meet the application of road scenarios. It is very easy to have the problem of missed vehicle detection and misdetection. To address this problem, this paper uses the Soft-NMS algorithm to replace the NMS algorithm to alleviate the problem of missed detection and false detection on dense target detection. It only needs to make simple changes to the traditional NMS algorithm, does not add extra parameters, has the same algorithm complexity as the traditional NMS, and is efficient.

The traditional NMS algorithm sets all the scores of the boxes with IOU greater than the threshold N_t to 0, meaning that they are directly deleted. I.e:

$$s_i = \begin{cases} s_i & iou(M, b_i) < N_t \\ 0 & iou(M, b_i) \geq N_t \end{cases} \tag{25}$$

where b_i denotes the remaining prediction frames with lower scores, which are the pending frames, M the current highest scoring frames, and s_i the frames left after NMS processing.

In contrast, in Soft-NMS algorithm, the scores of the boxes with CIOU greater than the threshold are attenuated, not directly suppressed, by means of a $f\left(iou\left(M,b_i\right)\right)$ weighting function. There are two main forms of weighting function, i.e., linear weighting and Gaussian weighting, and the idea of improvement is that the larger the CIOU with the current highest score M is, the more the score of the predicted box decreases. The two weighting formulas are:

$$s_i = \begin{cases} s_i & iou\left(M,b_i\right) < N_t \\ s_i\left(1 - iou\left(M,b_i\right)\right) & iou\left(M,b_i\right) \geq N_t \end{cases} \tag{26}$$

$$s_i = s_i e^{-\frac{iou\left(M,b_i\right)^2}{\sigma}}, \forall b_i \notin D \tag{27}$$

4.1.3. Loss function design of the model. In deep learning, a detection model has an objective function, and the process of running detection on the model is actually operating on the objective function. Usually in the detection of the model classification identification and regression process, the loss function is used as the objective function. The purpose of the loss function is to evaluate the error between the predicted value obtained after running the network model and the actual value of the experimental data. When the loss function is smaller, the error between the predicted value and the actual value is smaller, which indicates the better performance of the model.

In this paper, during the training of vehicle target detection model based on YOLOv5s algorithm, the multi-task loss function is used and its functional expression is:

$$L = L_{cls} + L_{box} + L_{rc} + L_{rb} \tag{28}$$

where L_{cls} is the target classification loss function, L_{box} is the prediction frame regression loss function, L_{rc} is the RPN classification loss function, and L_{rb} is the RPN bounding box regression loss function.

1) Target classification loss function and RPN network classification loss. The logarithmic loss function is used for classification and the logarithmic function predicts the probability value of the input between 0 and 1. It is used in multilevel classification to determine the loss. To wit:

$$L_{cls}\left(p_i, p_i^*\right) = -\log\left[p_i^* p_i + \left(1-p_i^*\right)\left(1-p_i\right)\right] \tag{29}$$

where the candidate region number is denoted as i, the target probability of candidate region i is denoted as p_i, and the positive and negative samples are denoted by p_i^*. If the positive sample probability p_i^* is 0, the probability of the negative sample is 1, and if the positive sample probability p_i^* is 1, the probability of the negative sample is 0. The value of the intersection and concatenation ratio IOUs between the predicted candidate region frame and the real frame is calculated, and when $IOU > 0.7$ the target probability p_i^* is 1, and when $IOU < 0.3$ the target probability p_i^* equals 0.

2) Prediction frame regression loss function and RPN bounding box regression loss function. In the bounding box regression problem there are two kinds of loss functions, $L1$-paradigm and $L2$-paradigm. Among them, the $L1$-paradigm loss function is used because the $L2$-paradigm weight will reconsider the oversize problem during the processing of discrete points, and the segmentation function with range $\left(-1,+1\right)$ is added to the $L1$-paradigm in order to make the loss function smoother and has the best smoothing near the 0 point.

For the border loss function L_{box}, $smooth_{L1}$ is used as a measure. The formulas for L_{box} and $smooth_{L1}$ are denoted as:

$$L_{box}\left(t_i,t_i^*\right)=\sum_{i\in\{x,y,w,h\}} smooth_{L1}\left(t_i,t_i^*\right) \tag{30}$$

$$smooth_{L1}\left(x\right)=\begin{cases}0.5x^2 & |x|<1\\ |x|-0.5 & |x|\geq 1\end{cases} \tag{31}$$

4.2. Statistics on the number of electric vehicles carried by roll-on/roll-off passenger ships

4.2.1. Comparative experiments with different models. After the experiment is completed, the results need to be analyzed using some metrics to judge the quality of the training model. The metrics that are commonly used in the process of multi-target detection at present are Average Precision (AP), Mean Accuracy of All Classes (mAP), Model Size (Params), and Frames per Second Transmission (FPS). For example, the fire pictures of EVs carried by passenger ships under different fire conditions obtained from the fire dynamics simulation, a total of 428 pictures of EVs on different passenger ship decks were acquired and made into a dataset to verify the model's effectiveness in this paper.

1) Ablation experiment. This paper is based on the YOLOv5s network, and the optimization of the Neck layer and the output end is used to carry out the target detection of electric cars after the fire. To verify the effectiveness and necessity of each module in this model, YOLOv5s is used as the benchmark, mAP value, model size, and FPS are used as the evaluation indexes, and the improvement modules are added gradually for ablation experiments. The experimental results are shown in Table 1.

(1) Algorithm B changes the original backbone network of YOLOv5s to a lightweight backbone network, ShuffleNetV2, which reduces the model size parameter by 45.59% and improves the number of transmitted frames per second by 30.65%, while the mAP is reduced by 3.87%. The experimental results show that using ShuffleNetV2 as the backbone network drastically reduces the model parameters and improves detection speed compared to Algorithm A.

(2) Algorithm C replaces the original PANet feature fusion network with the BiFPN network based on the ShuffleNetV2 backbone network. The mAP is improved by 2.22% compared with Algorithm B, which shows the effectiveness of the BiFPN network. In this experiment, BiFPN can fuse vehicle features better to improve detection accuracy.

(3) Algorithm D incorporates the ECA-Net attention mechanism into the ShuffleNetV2 network based on Algorithm C to create a new backbone network, ECAShuffle-Net, which improves the mAP by 2.89% compared to Algorithm C. The number of parameters is almost unchanged, which suggests that the ECA-Net can be more focused on extracting useful information from the features and does not increase network parameters.

(4) Algorithm E replaces the original algorithm's GIoU bounding box loss function with CIoU in the training phase. Compared to Algorithm D, mAP improves by 1.22%, proving that the CIoU loss function allows the model to exhibit better bounding box regression performance and obtain higher-quality anchor frames.

Table 1. The comparison of ablation experiment

Method	Backbone	Neck	Loss	mAP (%)	Params (M)	FPS
A	CSPdarknet	PANet	GIoU	94.02	7.15	62
B	ShuffleNetV2	PANet	GIoU	90.15	3.89	81
C	ShuffleNetV2	BiFPN	GIoU	92.37	4.08	78
D	ECAShuffle-Net	BiFPN	GIoU	95.26	4.12	75
E	ECAShuffle-Net	BiFPN	CIoU	96.48	4.23	83

2) Comparison test of different models. The performance of the YOLOv5s model proposed in this paper is compared with other advanced detection models, including the one-stage representative models Faster R-CNN, Mask R-CNN, and the two-stage representative models SSD and YOLOv5s. The same dataset is selected to ensure the fairness of the comparison experiments, and each detection model is trained separately. The experimental results are shown in Table 2.

Comparing the other advanced models, it is found that SSD, as an early one-stage algorithm, has the lowest mAP of only 83.78% because it is a one-stage detection model, so it has a significant advantage in detection speed compared to the two-stage Faster R-CNN, Mask R-CNN.YOLOv5s integrates a number of excellent algorithms and has a notable performance in both detection accuracy and speed. FasterR-CNN Mask R-CNN is weaker than the one-stage detection model in terms of detection speed due to the inherent disadvantage of the two-stage algorithm. In this paper, YOLOv5s is targeted to be improved according to the actual scene requirements, and the improved YOLOv5s model reaches the highest in both mAP and FPS, with values of 96.67% and 79, respectively, which illustrates the effectiveness of this paper's improvement of the YOLOv5s detection algorithm. By applying it to the target detection after the fire of electric vehicles carried by a passenger ship, it can distinguish the vehicle situation well under different degrees and provide support for the number of statistics on electric vehicles.

Table 2. Comparison of different models

Model	AP (%)			mAP (%)	FPS
	Car	SUV	MPV		
Faster R-CNN	86.17	85.64	84.73	85.51	34
Mask R-CNN	88.75	84.23	84.65	85.88	27
SSD	84.28	83.15	83.92	83.78	45
YOLOv5s	94.35	94.57	94.51	94.48	63
Ours	96.49	97.42	96.18	96.67	79

4.2.2. Counting of Electric Vehicles Carried by Rolling Stock Vessels/ In this paper, the model of a passenger ship carrying electric vehicles has 13 layers, and the loading of electric vehicles is mainly concentrated in layers 5 to 13. In this paper, a total of 428 images of passenger ships carrying electric vehicles after fire simulation are obtained, and 10 images are randomly selected from them. The model of this paper is compared with the traditional YOLOv5s algorithm, and the statistical results of the model's number of electric vehicles in different images are shown in Fig. 8. Shown.

The number of vehicles in the first set of images is 71, and the number of vehicles detected by the traditional YOLOv5s target detection algorithm is 57, while the number of vehicle counts obtained by this paper's model is 69. The accuracy of the statistical results of the number of electric vehicles carried by passenger ships obtained by the model of this paper is 92.96%. It can be seen that the traditional YOLOv5s target detection algorithm has a large error in counting the vehicles in the case of fire in the passenger-roller ship carrying electric vehicles. In contrast, the model in this paper is of higher accuracy. It can deal with the problem of counting the vehicles of the passenger-roller ship carrying electric vehicles in the case of fire more efficiently. It can obtain a more accurate counting result of the number of vehicles. The model in this paper can solve the problem of inaccurate counting of vehicles by the target detection method due to too many fire-damaged vehicles and can better obtain the number of fire-damaged electric vehicles and measure the loss of the electric vehicles carried by the passenger ship after the fire.

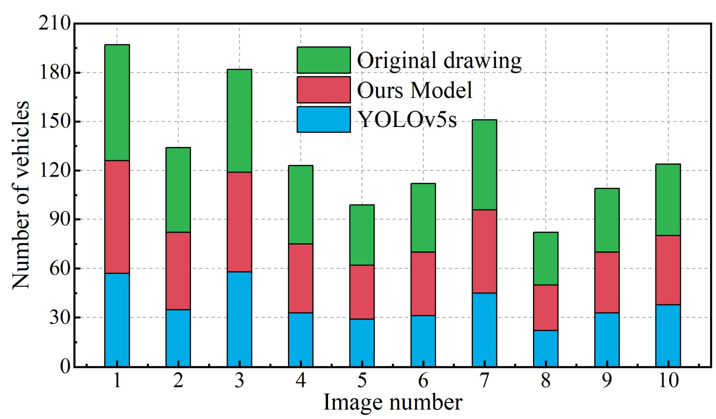

Fig. 8. Statistics on the number of electric cars

5. Conclusion

Based on FDS software, the article simulates the damage of electric vehicles carried by passenger-roller ships under fire conditions. It combines the improved YOLOv5s model for the target detection of electric vehicles after the fire to calculate the number of electric vehicles. Under the fire condition, when the external ambient wind speed increases from 0.5m/s to 6.5m/s, the maximum temperature at the fire center of the passenger-roller ship carrying EVs decreases from 883.93℃ to 748.57℃. The higher the fire intensity is, the higher the maximum temperature at the deck center of the passenger-roller ship increases continuously, from 486.83℃ to more than 932.76℃. When the firepower reaches 800kW, the peak temperature of the smoke layer can reach 144.0℃, and the firepower is positively correlated with the air layer temperature in the cabin under the same conditions. The improved YOLOv5s model has the highest mAP of 96.67% for EV target detection after fire damage, and the statistical accuracy for the number of EVs after fire reaches 92.96%. Based on the destruction pictures of EVs carried by a passenger ship obtained from fire dynamics simulation, relying on deep learning technology can effectively detect EVs and provide support for realizing the number calculation of EVs.

In this paper, although the number of EVs carried by a passenger-roller ship is solved under fire dynamics simulation, it is mainly from the perspective of target detection, which is the detection of static images, while the fire occurrence process is more of a dynamic process. In subsequent studies, the dynamic detection of EVs needs to be further optimized to reduce the maximum loss of EVs under the fire conditions of a passenger-roller ship.

References

[1] Banaei, M., Ghanami, F., Khooban, M. H., & Boudjadar, J. (2021, August). Cost-effective control of Roll-on/Roll-off Emission-Free Ships. In 2021 25th International Conference on Methods and Models in Automation and Robotics (MMAR) (pp. 315-320). IEEE.

[2] Melideo, D., & Desideri, U. (2024). The use of hydrogen as alternative fuel for ship propulsion: A case study of full and partial retrofitting of roll-on/roll-off vessels for short distance routes. International Journal of Hydrogen Energy, 50, 1045-1055.

[3] Angraini, N. (2022). THE EFFECT OF SERVICE QUALITY ON USER SATISFACTION OF ROLL ON ROLL OFF (RO-RO) SHIPS. Jurnal Ekonomi, 11(01), 310-320.

[4] Ančić, I., Vladimir, N., & Luttenberger, L. R. (2018). Energy efficiency of ro-ro passenger ships with integrated power systems. Ocean Engineering, 166, 350-357.

[5] Alisafaki, A. G., & Papanikolaou, A. D. (2017). On the energy efficiency design index of RO-RO passenger and RO-RO cargo ships. Proceedings of the Institution of Mechanical Engineers, Part M: Journal of Engineering for the Maritime Environment, 231(1), 19-30.

[6] Szymoński, M., & Mariner, M. (2019, April). Some notes on risk and safety evaluation of Ro-Ro passenger ships exploitation. In 2019 European Navigation Conference (ENC) (pp. 1-6). IEEE.

[7] Szymoński, M. (2024). Safety Management on Ro-Ro Passenger Ships. TransNav, International Journal on Marine Navigation and Safety od Sea Transportation, 18(2), 281-285.

[8] Wang, X., Liu, Z., Loughney, S., Yang, Z., Wang, Y., & Wang, J. (2022). Numerical analysis and staircase layout optimisation for a Ro-Ro passenger ship during emergency evacuation. Reliability Engineering & System Safety, 217, 108056.

[9] Wang, X., Liu, Z., Zhao, Z., Wang, J., Loughney, S., & Wang, H. (2020). Passengers' likely behaviour based on demographic difference during an emergency evacuation in a Ro-Ro passenger ship. Safety science, 129, 104803.

[10] Wahyuni, T., Ricardianto, P., Harits, A., Thamrin, M., Liana, E., Anggara, D., ... & Endri, E. (2022). The implementation of minimum service standards on ship operational performance: Empirical evidence from Indonesia. Uncertain Supply Chain Management, 10(4), 1297-1304.

[11] Rahmanita, M., Ricardianto, P., Wijayanti, R., Agusinta, L., Asmaniati, F., Djati, S., ... & Endri, E. (2023). The impact of the safety of passenger ship services on the development of water recreation: evidence from Indonesia. Uncertain Supply Chain Management, 11(3), 1121-1132.

[12] Akpudo, C. U. (2021). Trend Analysis of Boat Accidents and Causes in the Waterways of Nigeria. Int. J. Sci. Res. in Multidisciplinary Studies Vol, 7(11).

[13] Gatti, R., Nandini, R. B., & Gagana, C. (2018, May). Boat Navigation and Safeguard of Passenger's Over Flood Disaster. In 2018 3rd IEEE International Conference on Recent Trends in Electronics, Information & Communication Technology (RTEICT) (pp. 2274-2277). IEEE.

[14] Abd Razak, M. F., Osnin, N. A., Rahman, N. S. F. A., Hamid, S. A., Kader, A., & Saman, A. (2017). Safety Assessment Of Passenger Boat And Houseboat At Temenggor Lake, Malaysia. Insight, 11.

[15] Kim, H. S., Cho, M. G., Kang, S. W., Kim, J. W., Pyo, C. M., Ji, C. W., & Park, J. I. (2023, June). Design and Simulation of Hinge-Type Ro-Ro (Roll-on/Roll-off) Ship Car Deck Structure. In ISOPE International Ocean and Polar Engineering Conference (pp. ISOPE-I). ISOPE.

[16] Somera, J. D. C., Parado, S. P. E., Castro, M. T., & Ocon, J. D. (2021). Techno-economics of hybrid system electrification of roll-on/roll-off vessels in the Philippines. Chemical Engineering Transactions, 88, 559-564.

[17] Aravind, K. R., & Sudheer, C. B. (2024, January). Revolutionizing Maritime Transport: A Blueprint for Sustainable Mobility-Conceptualizing an Electric Roll-On/Roll-Off (RO-RO) Ferry System for India's National Waterway 3. In Proceedings of the First International Conference on Science, Engineering and Technology Practices for Sustainable Development, ICSETPSD 2023, 17th-18th November 2023, Coimbatore, Tamilnadu, India.

[18] Jia, B., & Fagerholt, K. (2021). Step-wise stowage planning of roll-on roll-off ships transporting dangerous goods. Maritime Transport Research, 2, 100029.

[19] Hansen, J. R., Fagerholt, K., Stålhane, M., & Rakke, J. G. (2020). An adaptive large neighborhood search heuristic for the planar storage location assignment problem: application to stowage planning for Roll-on Roll-off ships. Journal of Heuristics, 26, 885-912.

[20] Jason Floyd & Daniel Madrzykowski. (2024). Fire dynamics simulator modeling of a line-of-duty death in a firefighting training facility using recent research on materials and firefighter safety. Journal of Fire Sciences(3),248-278.

[21] Vibha Sahu,Mohd Amin Khan & Omprakash D Madguni. (2024). Assessing forest fire dynamics and risk zones in Central Indian forests: a comparative study of the Khandwa and North Betul forest divisions of Madhya Pradesh. Environmental monitoring and assessment(9),810.

[22] Deyong Shang,Zhibin Lv,Zehua Gao & Yuntao Li. (2024). Lightweight detection model for coal gangue identification based on improved YOLOv5s. Journal of Real-Time Image Processing(4),137-137.

[23] Wei Wang,Xin Li,Xin Lyu,Tao Zeng,Jiale Chen & Shangjing Chen. (2023). Multi-Attribute NMS: An Enhanced Non-Maximum Suppression Algorithm for Pedestrian Detection in Crowded Scenes. Applied Sciences(14).